Composites Part B 161 (2019) 411–426

Contents lists available at ScienceDirect

Composites Part B

journal homepage: www.elsevier.com/locate/compositesb

Experimental and numerical evaluation of fiber-matrix interface behaviour of different FRCM systems

Alessandro Bellini[a], Marco Bovo[b,*], Claudio Mazzotti[b]

[a] CIRI Buildings and Construction (CIRI-EC), University of Bologna, Via del Lazzaretto 15/5, 40131, Bologna, Italy
[b] Department of Civil, Chemical, Environmental and Materials Engineering (DICAM), University of Bologna, Viale Risorgimento 2, 40136, Bologna, Italy

ARTICLE INFO

Keywords:
Carbon fibre
Glass fibres
Adhesion
Interface/interphase
Finite element model

ABSTRACT

Fiber Reinforced Cementitious Matrix (FRCM) composites are a relatively new strengthening system family, whose mechanical behavior is strongly affected by the wide array of possible inorganic matrices and composites fabrics that can be used and coupled together. Structural tests highlighted that global capacity of the system is strongly affected by fabric-matrix adhesion mechanism. In the present paper, the experimental results of tensile and single-lap shear tests, aimed to define mechanical properties of four FRCM types, are discussed and compared. For each system type, the failure modes for both types of test have been physically identified and clarified. The following development of detailed finite element models, carefully reproducing the mechanical behavior of the different layers of the strengthening system, allowed for the proposal of a reliable shear stress-slip relation for the fiber-matrix interface. The experimental outcomes showed the relevant dispersion of the results in terms of performance, effectiveness and failure mechanisms exhibited by the different FRCM types while the numerical interpretation allowed for a better understanding of the reasons and the parameters behind them.

1. Introduction

In the last decades, the growing need for repair and rehabilitation of existing buildings boosted the research of innovative restoration and strengthening techniques. In this framework, Fiber Reinforced Cementitious Matrix (FRCM) represents an innovative and effective retrofitting system. It is characterized by some promising features such as better compatibility with the substrate, vapor permeability, fire resistance, reversibility, applicability on wet surfaces, reduced times and costs of installation and durability [1], which often made it preferable to other reinforcement techniques (e.g. FRP), also in view of sustainability of intervention.

Even though several studies are currently available concerning the tensile behavior and bond performance of FRCMs [2–8], some fundamental mechanisms are still to be comprehensively clarified. Among these, one of the most relevant, but at the same time not completely identified, concerns the description of force transfer between the various layers of the reinforcement, while the reinforcement-substrate interface is usually much stronger [9] and provides for a negligible contribution to the deformation of the whole strengthening system [10,11]. In fact, if in FRP composite materials the most common failure mode is debonding from the substrate with detachment of a thin layer of material [12–19], FRCM systems typically show different and much more complex failure modes, influenced by mechanical properties, geometry and type of grid and mortar [20–23]. Several experimental analyses have been carried out to characterize the bond behavior of FRCM systems applied to both concrete and masonry substrates [24–28]. The observed failure modes (see Fig. 1) collected from an overview of the existing literature have been:

- debonding inside the substrate with detachment of a thin layer of substrate and of the entire FRCM strip (I);
- debonding at FRCM-substrate interface with detachment of the entire composite (II);
- debonding at the fiber-matrix interface with delamination of the inner layer of mortar (III);
- purely fiber slippage within matrix layers (IV);
- fiber slippage within the matrix layers with cracking of the outer layer of mortar (V);
- tensile failure of the fiber out of the bonded region (VI).

As an outcome emerging from a wide literature review [3,4,29], the authors found that a common failure mode, described by several authors, is the type III: debonding at the fiber-matrix interface. It is typically characterized by delamination of the reinforcement from the mortar of the inner layer also coupled to minor slippage and

* Corresponding author.
E-mail address: marco.bovo@unibo.it (M. Bovo).

https://doi.org/10.1016/j.compositesb.2018.12.115
Received 14 August 2018; Received in revised form 30 November 2018; Accepted 28 December 2018
Available online 30 December 2018

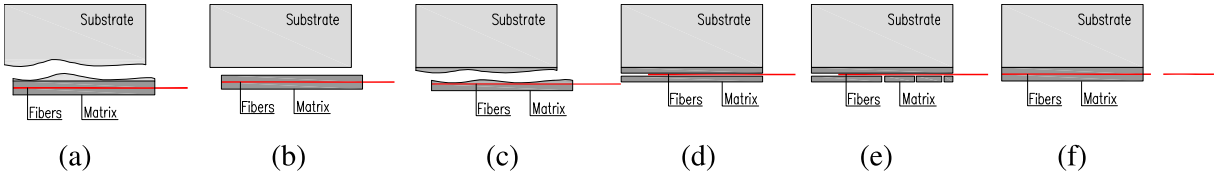

Fig. 1. Most typical failure modes observed for FRCM: (a) Debonding inside the substrate with detachment of a thin layer of substrate and entire FRCM strip; (b) Debonding at FRCM-substrate interface with detachment of the entire composite; (c) Debonding at the fiber-matrix interface; (d) Purely fiber slippage within matrix layers; (e) Fiber slippage within the matrix layers with cracking of the outer layer of mortar; (f) Tensile rupture of the fiber out of the bonded surface.

deformation of the longitudinal fiber bundles. Moreover, it was found that the type of failure mechanism is strongly dependent from the type of fiber grid adopted for the reinforcement preparation [21,22]. However, the addiction of other components, such as, for example, an adhesion promoter, together with the modification of some mechanical properties of the mortar used as a matrix [30] can considerably change the maximum debonding load and the expected failure modes of the samples when subjected to bond tests.

In this framework, the present paper mainly focuses on the role played by fiber-matrix interface in defining the tensile and bond behavior of different types of FRCM systems. The problem has been investigated experimentally and then the experimental tests have been numerically modelled in order to better identify the shape of reliable interface laws and their role.

In more details, specimens constituted of bi-directional glass and carbon grids and natural hydraulic lime (NHL) mortars were prepared and tested under tensile tests or applied on masonry panels and tested under single-lap shear tests. Four different types of FRCM systems, based on dry carbon fibers, coated glass fibers or on glass and carbon fibers applied with the addition of an adhesion promoter, were tested in the experimental campaign. In order to analyze a wide scenario of different failure modes cracks propagation and adhesion mechanisms, the four different systems were selected because considered as limit cases in the range of the current FRCM applications.

A further aspect investigated during experimental tests was the definition of the mortar tensile strength by adopting two different type of tests: tensile and flexural tests. The corresponding strengths were compared and interesting results emerged in view of the setting up of a characterization protocol to be adopted for the certification of FRCM systems.

In order to analyze the tensile and shear behavior of the different FRCM classes, detailed finite element (FE) models were created to carefully reproduce the mechanical behavior of the various layers of the strengthening systems, allowing for a better understanding of the various experimental scenarios. In particular, for each type of reinforcements the FE model included a detailed modelling of the two layers of matrix, of the composite glass or carbon grid and of the matrix-fiber interface. At a material level, to introduce inside the FEM a random crack pattern (connected to tensile strength variability of the matrix mortar); five different matrix mortar classes were defined following a Poisson distribution for their tensile strength. Then, local τ-slip relations were indirectly evaluated and calibrated against global force-slip curves coming from considered bond tests. The obtained relations were also compared with analytical relations existing in literature. Finally, after introducing the matrix properties and the interface laws inside the FE models, their reliability was verified against the force-elongation curves coming from the tensile tests.

The analysis carried out clarified the importance of the different aspects of the interface laws and suggested the role of the fiber bundles orthogonal to the applied force during the bond tests.

The presented results will also contribute to the collection of an extended database of results for describing the mechanical behavior of FRCM composites.

2. Materials characterization and test set-UPS

2.1. Experimental program, materials characterization and samples preparation

The present experimental campaign focuses on the analysis of the tensile and bond behavior of four different types of FRCM composites applied on masonry substrate. Carbon FRCM (CFRCM) and Glass FRCM (GFRCM) strengthening systems, characterized by bi-directional grid embedded inside natural hydraulic lime mortar, were tested. A total of 20 tensile tests and 20 bond tests (i.e. 5 repetitions for each of the four groups) were carried out.

In order to investigate the bond behavior of the reinforcements, masonry panels composed of five clay bricks (with dimensions $250 \times 120 \times 55\ mm^3$) spaced by lime mortar joints about 10 mm thick were prepared. The bricks adopted are fired clay bricks produced by compaction, with mechanical properties similar to those of existing clay bricks constituting historical buildings [31]. They were characterized by performing, on samples extracted by the bricks, compressive and flexural tests along directions perpendicular and parallel to the bed face [32]. Mechanical properties of NHL mortar used for masonry panels (NHL_m) and for strengthening systems (NHL_r) were defined according to UNI EN 1015–11:2007 [33]. Results obtained from materials characterization are summarized in Table 1.

Four different types of balanced bi-directional fiber grids were adopted in the study:

- the first grid was based on dry carbon fibers with a strand spacing of 9 mm and a density of 170 g/m^2 (with an equivalent dry fiber thickness of 0.047 mm), and was applied by using an adhesion promoter (CP group of specimens);
- the second one, based on uncoated glass fibers with a nominal spacing of 12 mm, a density of 300 g/m^2 and an equivalent dry thickness of 0.060 mm, again applied together with an adhesion promoter (GP group of specimens);
- the third grid, based on dry carbon fibers with a density of 170 g/m^2 and a spacing of 20 mm with equivalent dry fiber thickness 0.047 mm, was used for preparation of CD group of specimens;
- the fourth strengthening system, based on coated glass fibers with a density of 300 g/m^2, a nominal spacing of 18 mm and an equivalent thickness of 0.055 mm, was used in GC group of samples.

CP and GP samples have $NHL_{r,1}$ mortar, whereas for CD and GC

Table 1
Materials characterization of bricks and mortars adopted in the experimental tests (average values).

Material	Compressive strength f_c [MPa]	Flexural strength $f_{t,flex}$ [MPa]	Splitting tensile strength $f_{t,split}$ [MPa]
Brick (⊥ bed)	18.59	4.66	2.59
Brick (// bed)	23.05	4.86	3.14
NHL_m mortar	6.01	2.76	–
$NHL_{r,1}$ mortar	9.83	3.84	–
$NHL_{r,2}$ mortar	16.07	5.82	–

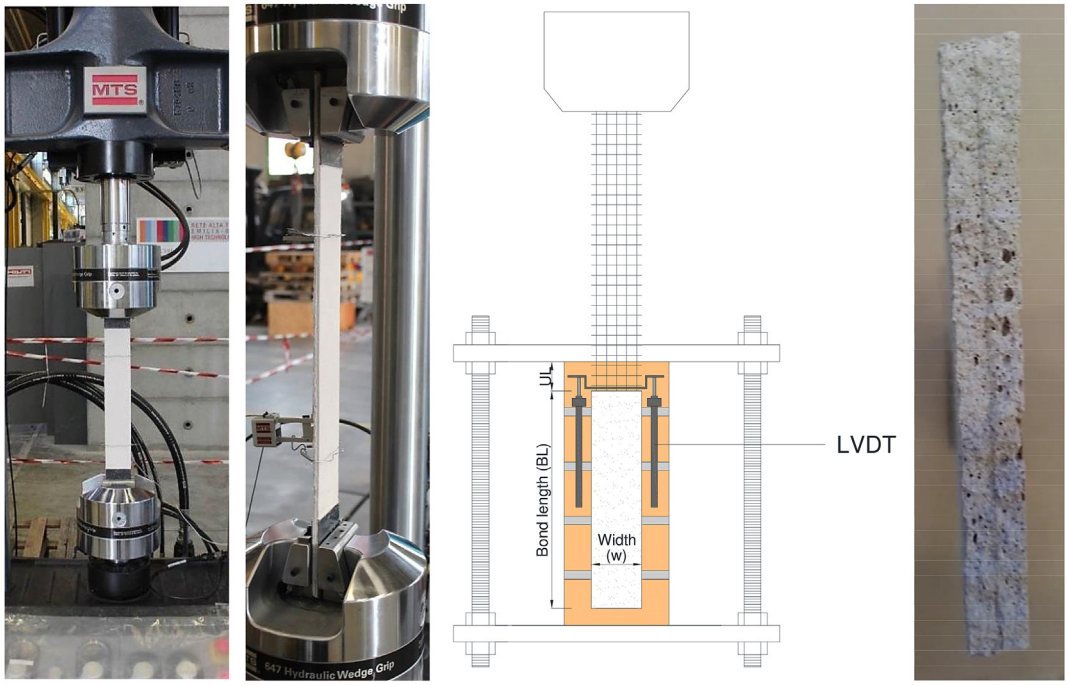

Fig. 2. Experimental set-up and view of results of tensile tests on unreinforced mortar coupons: (a) tensile tests; (b) single-lap shear tests; (c) view of defects on mortar matrix detected at the end of tensile tests.

specimens, $NHL_{r,2}$ mortar was used. Tensile strength and elastic modulus of the various grids are respectively: 2200 MPa and 240 GPa (CP samples), 1000 MPa and 65 GPa (GP samples), 1900 MPa and 240 GPa (CD samples), 1055 MPa and 70 GPa (GC samples). An adhesion promoter, developed in order to improve the fiber-matrix adhesion capacity, was used for CP and GP groups of samples. The promoter is a two-component, water-based product, consisting of two resins supported on an inorganic, microcrystalline, thixotropic matrix, characterized by a flexural strength of 5 MPa, an elastic modulus of 4.5 GPa and an ultimate deformation of 1.2%.

FRCM strengthening systems subjected to tensile test (Fig. 2a) and bond test (Fig. 2b) were prepared, for each group, by using the same materials, the same geometry and the same thickness, in order to analyze and compare homogeneous results. The reinforcement width (w in Fig. 2b) was chosen as an integer multiple of the grid spacing in order to include at least 4 longitudinal bundles. The adopted reinforcement width was 54 mm for CP samples (6 yarns included), 60 mm for GP samples (5 yarns), 80 mm for CD specimens and 72 mm for GC specimens (i.e. 4 yarns included for these last two groups). Thickness of the two mortar layers of the reinforcement systems was controlled by using, during the casting, appropriate spacers 3 mm thick (for a total mortar thickness $t = 6$ mm). Before the application of the reinforcement system, the masonry substrate was prepared trough brushing, cleaning and wetting of the surface.

The adhesion promoter, when present, was applied above the first mortar layer before placing the composite grid and then above the grid before the application of the upper mortar layer.

A bond length (BL in Fig. 2b) of 260 mm was chosen for all the specimens subject to single-lap shear test, after an unbonded length (UL in Fig. 2b) of 30 mm, measured from the front side of the samples. Specimens for tensile tests were prepared according to the same procedure and adopting the geometry (t and w) already described, but with a total length of 500 mm.

2.2. Tensile tests

Specimens were strengthened at their extremities by using composite tabs and, by means of the hydraulic clamping system, an appropriate pressure was chosen in order to prevent damage to the specimen edges and to avoid slippage phenomena. Tests were performed by using a MTS hydraulic testing machine under displacement control at a rate of 0.1 mm/min during the un-cracked phase and of 0.2 mm/min during the cracked phase. Longitudinal strain in the central portion of the samples was measured by using a MTS extensometer, with a gage length of 200 mm. A view of the experimental set-up is reported in Fig. 2a.

2.3. Bond tests

The experimental single-lap set-up used for bond tests is shown in Fig. 2b. Samples were placed in a rigid steel frame, fixed on the lower grips of a MTS hydraulic testing machine (the same used for tensile tests), characterized by a maximum capacity of 100 kN. In order to promote a correct transverse distribution of the applied force among the different bundles, the loaded extremity of the FRCM reinforcement was impregnated with epoxy resin and then clamped by the wedges of the testing machine.

Tests were performed under displacement control, by imposing a rate of 0.15 mm/min. Two 20 mm displacement transducers (LVDTs) were used to measure the relative displacement (i.e. the total slip) between the reinforcement and the substrate (see Fig. 2b).

2.4. Useful remarks on the tensile strength of the reinforcement mortar

In order to properly evaluate the tensile strength of the mortar used as matrix within FRCM reinforcement (i.e. NHL_r mortar), so to accurately define the parameters adopted in the numerical models, direct tensile tests on two-layers mortar coupons prepared without reinforcement grid have been carried out, using the same set-up adopted for tensile tests on FRCM specimens. Results have been compared with

Table 2
Comparison between the tensile strength of the reinforcement mortar obtained by means of different test types.

Material	Test protocol	Test type	Tensile strength f_t [MPa]	CoV [%]	Ratio $f_{t,flex}/f_{t,tensile}$
$NHL_{r,1}$ mortar	UNI EN 1015–11:2007	Flexural test ($f_{t,flex}$)	4.20	15.3	2.09
	Tensile test on FRCM (see Section 2.2)	Pure tensile test ($f_{t,tensile}$)	2.01	11.6	

those found by conventional test methods typically adopted for mortar materials characterization (i.e. three-point bending tests on prisms). To this purpose, by using $NHL_{r,1}$ mortar, 10 coupons $6 \times 60 \times 500\,mm^3$ and 10 standard prisms $40 \times 40 \times 160\,mm^3$ were prepared and then tested after a curing period of 28 days. Results obtained by the two different types of test are summarized in Table 2.

As expected, the flexural strength $f_{t,flex}$ obtained according to UNI EN 1015-11 via three-point bending test is about two times higher than the tensile strength $f_{t,tensile}$ obtained through direct tensile tests on the coupons.

The obtained results can be explained by considering the different role played by the unavoidable defects (see the air bubbles in Fig. 2c) located inside specimens of different thickness (about 6 mm for mortar coupons *vs* 40 mm for standard prisms) and with different stress distributions (due to different test methods). These preliminary results could open a debate on the most suitable tests to be adopted for the mechanical characterization of mortar matrix, also in view of a standardization of materials qualification procedure and certification process. The subject is not addressed here for reason of space and clarity of purpose but will be object of future researches.

3. Experimental results

3.1. Tensile tests

The main results are reported in terms of failure modes and stress-strain diagrams for the four different types of FRCM strengthening systems. In particular, the stress is considered as the ratio between the applied load and the area of longitudinal dry fibers while strain was measured by means of an extensometer located in the central part of the sample, as shown in Fig. 2a. Table 3 shows the elastic moduli characterizing the different branches of the diagrams. In addition, the parameter $\varepsilon_{lim,conv}$, intended as the conventional limit strain corresponding to bond tests, has been reported. It was calculated as the ratio between characteristic stress value emerging from bond tests and elastic modulus of dry fibers of the strengthening systems, according to the recent CNR-DT 215 guidelines on the design of FRCM interventions [34]. The observed failure modes were (I) tensile failure inside the gage length of the extensometer or (II) fiber rupture outside the gage length in proximity of the tabs (see Fig. 3).

3.1.1. CP reinforcement

CP samples (Fig. 4a) showed a typical trilinear behavior with continuous transition between the different branches. During the tests, the cracking pattern observed along the specimens was characterized by a number of very small and distributed cracks finally leading to the formation of a critical crack. The transition between following branches was smooth due to the presence of the adhesion promoter and with low scattering of results, if compared with those obtained without the adhesion promoter (see Table 3). As a remark, third phase elastic modulus (E_3) is very similar to the elastic modulus of dry carbon fibers, confirming that, along the final branch, only the reinforcement grid was effective.

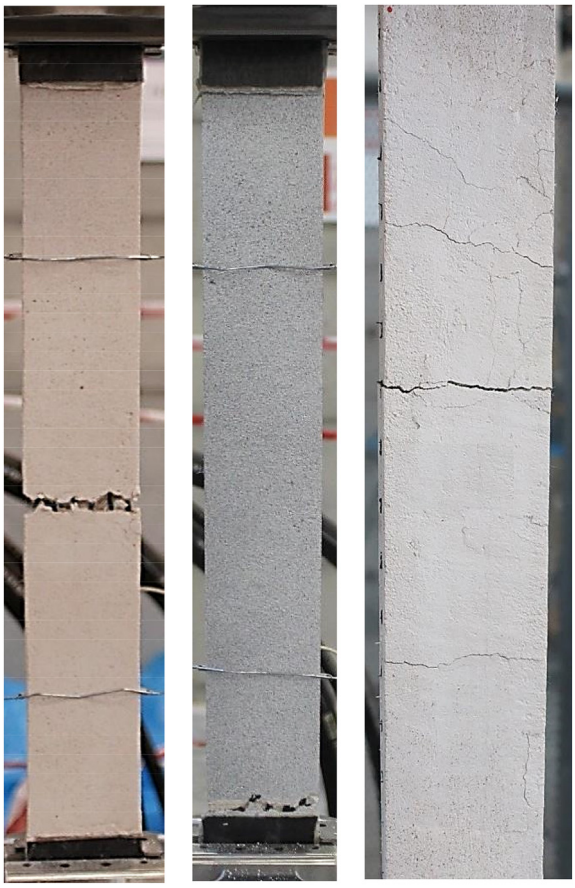

Fig. 3. Failure modes identified during tensile tests: (a) Failure mode I (tensile failure inside the gage length of the extensometer); (b) Failure mode II (fiber rupture outside the gage length); (c) Example of matrix disaggregation.

Table 3
Mechanical parameters describing the tensile behavior of FRCM samples.

Sample type		σ_1 [MPa]	σ_2 [MPa]	σ_u [MPa]	ε_1 [%]	ε_2 [%]	ε_u [%]	E_1 [GPa]	E_2 [GPa]	E_3 [GPa]	$\varepsilon_{lim,conv}$ [%]	Failure mode
CP	Average	203	1359	2530	0.051	0.638	1.137	410	197	234	0.534	I - II
	CoV [%]	9.9	5.5	5.0	17.0	7.1	4.4	18.6	2.1	3.1		
GP	Average	125	–	1165	0.055	–	1.542	236	–	70	1.038	II
	CoV [%]	6.0	–	3.2	20.2	–	2.4	19.0	–	4.5		
CD	Average	310	–	1290	0.019	–	0.701	1687	–	190	0.120	I - II
	CoV [%]	35.0	–	6.9	20.0	–	10.2	34.9	–	13.9		
GC	Average	127	199	854	0.009	0.345	1.539	1420	22	56	0.599	I - II
	CoV [%]	26.1	13.3	2.9	14.2	19.8	8.5	33.2	54.6	6.6		

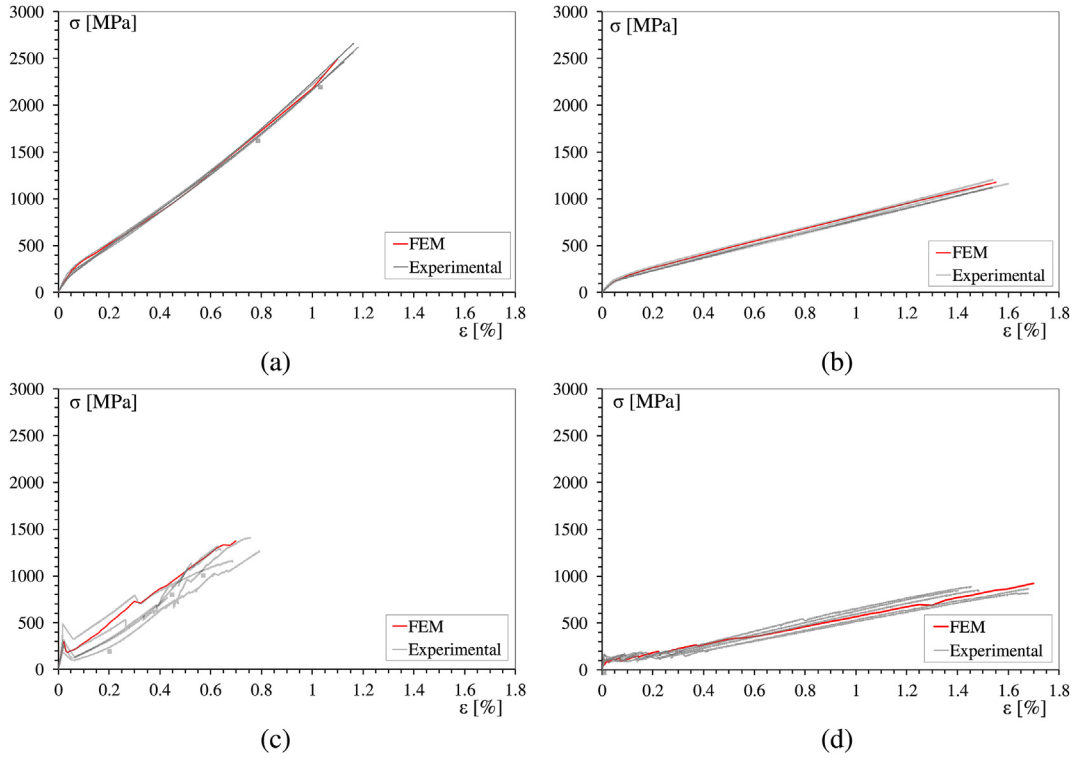

Fig. 4. Stress-strain graphs coming from tensile test on FRCM strengthening systems and comparison with numerical (FEM) model: (a) CP specimens; (b) GP samples; (c) CD specimens; (d) GC samples.

Table 4
Main experimental results from bond tests.

Sample type	Failure mode (recurring of mechanism)	Average maximum load [kN]	Average ultimate stress (σ_f) [MPa]	CoV of σ_f [%]
CP	III(5)	3.838	1438	5.5
GP	III(1)-VI(3)-VI[a](1)	2.843	790	7.3
CD	IV(5)	1.182	314	3.9
GC	IV(3)-IV[b](2)	2.341	591	14.5

[a] Partial delamination before fiber tensile failure.
[b] Fiber slippage with final tensile failure of the reinforcement.

3.1.2. GP reinforcement

The tensile behavior of GP samples is shown in Fig. 4b. Stress-strain graphs show, unlike the previous case, a typical bilinear behavior, where the second and third branches became a single, almost linear, branch until failure. As for CP specimens, the use of an adhesion promoter led to the formation of very small and distributed cracks, with the corresponding smooth transition between the uncracked and the cracked phase.

3.1.3. CD reinforcement

CD specimens showed a large scattering of results, with a significant stiffness reduction after first cracking (Fig. 4c). The tension stiffening effect was not so apparent since the formation of few cracks rapidly increasing their opening, due to a noticeable fiber slippage and often matrix disaggregation, led abruptly to the third branch (see Fig. 3c). The elastic modulus of the third branch reported in Table 3, generally lower than that of carbon fibers, confirmed the presence of not negligible slippage phenomena.

3.1.4. GC reinforcement

The typical behavior of GC specimens is presented in Fig. 4d. Samples showed a trilinear behavior different from CP specimens, with a second cracked phase characterized by several evident small load drops, associated to new cracks opening, and a third almost linear branch where the stabilized cracks increased their width. Unlike GP samples, cracks were less distributed and were much more visible on the specimens, with some fiber slippage. As far as the tensile behavior of the samples is concerned (see Table 3), ultimate stress, strain and third branch elastic modulus (E_3) seem similar among tests repetitions, whereas E_1 and E_2 showed the largest variability.

3.2. Bond tests

In this section, bond failure modes, bond capacity and load-slip (*F*-slip) curves will be analyzed and discussed for the different types of FRCM strengthening systems tested. Slip is defined as the relative displacement between the beginning of the FRCM unbonded portion and the adjacent substrate. Table 4 shows bond capacity together with the identified failure mode (Fig. 5) for the specimens tested.

3.2.1. CP reinforcement

All CP specimens showed failure mode III: full delamination inside the lower mortar layer. This failure mode (Fig. 5a) is typical of carbon grids with a good fibers-matrix adhesion (due to the presence of an adhesion promoter) and occurred with the detachment of the carbon grid together with a thin mortar layer of the lower matrix, with the upper layer remaining attached to the grid. As before, the adhesion promoter led to a reduced statistical variation with a coefficient of variation (CoV) referred to the ultimate stress, which resulted lower than 6% (see Table 4). The load-slip curves reported in Fig. 6a are characterized by a first almost linear branch followed by a typical wavy sub-horizontal behavior, starting after the onset of the delamination process.

3.2.2. GP reinforcement

Two alternative failure modes were observed, characterized by tensile failure of the unbonded fibers (VI) (see Fig. 5b) or by partial

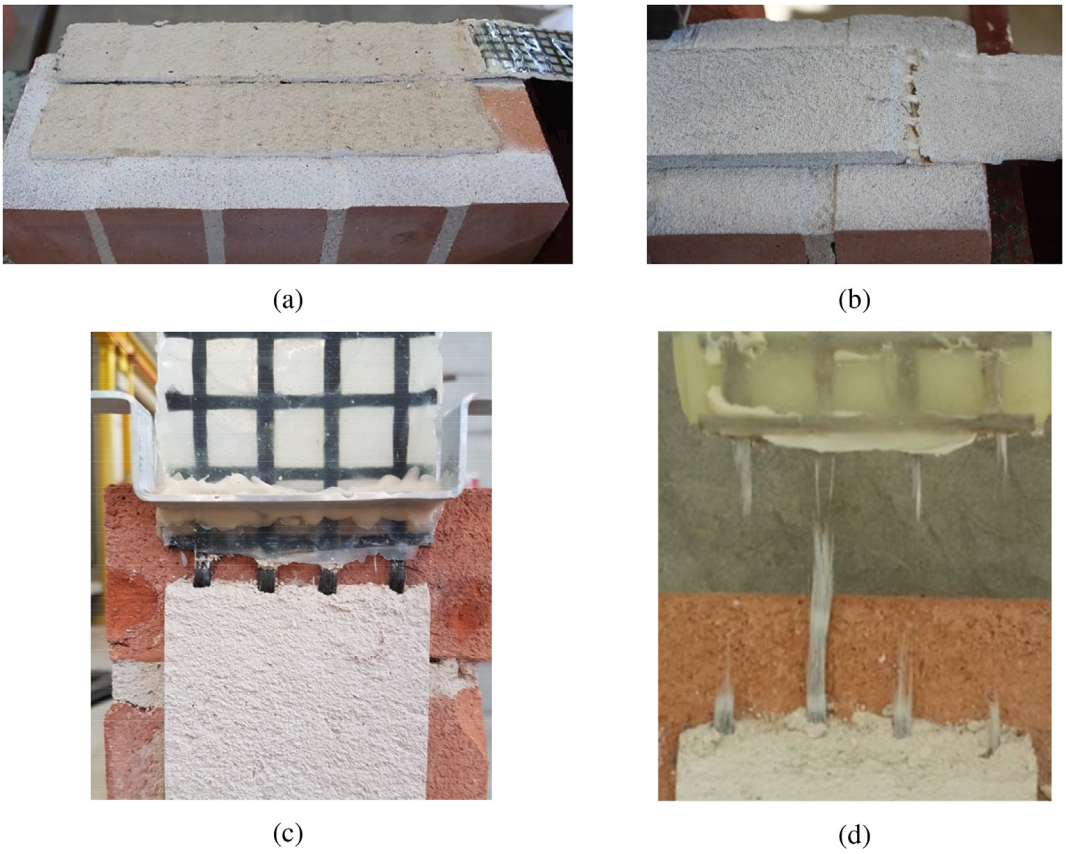

Fig. 5. Failure modes identified during bond tests: (a) Failure mode III (debonding for delamination of the inner mortar layer); (b) Failure mode VI (tensile rupture of the fibers in the unbonded region); (c) Failure mode IV (purely fiber slippage within the matrix layers); (d) Failure mode IV** (fiber slippage with final tensile failure).

(VI*) or full (III) delamination of the reinforcement. As for CP samples, the maximum bond capacity (or i.e. the ultimate stress) showed a reduced variability (CoV = 7%). Fig. 6b shows the typical bond behavior of GP samples, where, after the first almost linear branch, in most cases, there was a sudden failure or a limited sub-horizontal curve, corresponding to the tensile failure of the textile.

3.2.3. CD reinforcement

CD specimens are characterized by the use of dry carbon fibers without coating, which led to failure mode IV (Fig. 5c) and to an apparent fibers slippage inside the matrix. Repeatability of tests is good (CoV < 4%) even though the bond capacity is quite low. The analysis of load-slip curves in Fig. 6c shows a first linear branch followed by a softening branch, which is governed by fiber slippage. After large slips, a residual bond capacity can be observed due to fibers-mortar friction. For this type of dry grids, the transverse bundles seem not efficient and, after the breaking of the weak connections between the orthogonal bundles, they have a negligible influence on the slippage of the longitudinal dry carbon yarns.

3.2.4. GC reinforcement

GC samples are the only ones, among those considered, presenting fibers with an external coating, which is quite common on the market [21]. Typical failure mode revealed by this group of samples is again the # IV (slippage of the textile within the matrix as for CD samples), while in some cases, final fibers tensile failure also occurred (failure mode IV** showed in Fig. 5d).

Fig. 6d shows load-slip curves of GC specimens, which are characterized almost from the beginning by a nonlinear behavior. Fibers slippage probably started before the peak and took control of the test during the softening branch. For large slips, an important friction bond capacity was observed, even though the connections between orthogonal bundles were not so efficient. In order to confirm this aspect, after the bond test an accurate survey of the state of the transverse bundles was carried out by removing the outer matrix layer. Fig. 7a shows that transverse bundles are embedded exactly in their original position still wrapped by the two matrix layers and they do not follow the slippage of the longitudinal yarns. In Fig. 7 the original connections positions are the light gray spots on the longitudinal bundles indicated by the arrows. Moreover, the broken longitudinal bundles shown in Fig. 7b present in the failed portion a sawtoothed aspect maybe to be attributed to rubbing damage of fibers on the granular texture of matrix. This caused a premature failure of the bundle, even if for a low load value.

One of the bond tests was extended until the complete pullout of the longitudinal bundles (see Fig. 8). During the process, one of the bundles failed with a residual applied force about one-half of the peak-value. Analysis of the broken part suggested that frictional rubbing could have reduced the cross-section, thus explaining why, also for lower level of slip some bundles prematurely failed during the bond test.

4. Numerical interpretation and comparison with experimental results

4.1. Description of FE models

In order to understand the local behavior of the strengthening system components, a nonlinear finite element (FE) model was created, starting from the geometry of the real specimens. Due to the particular restraint and loading conditions prescribed during the experimental tests, the hypothesis of plane stress condition across the longitudinal section of the specimens was assumed for both the analysis of the tensile and bond behavior of the FRCM systems. In particular, for

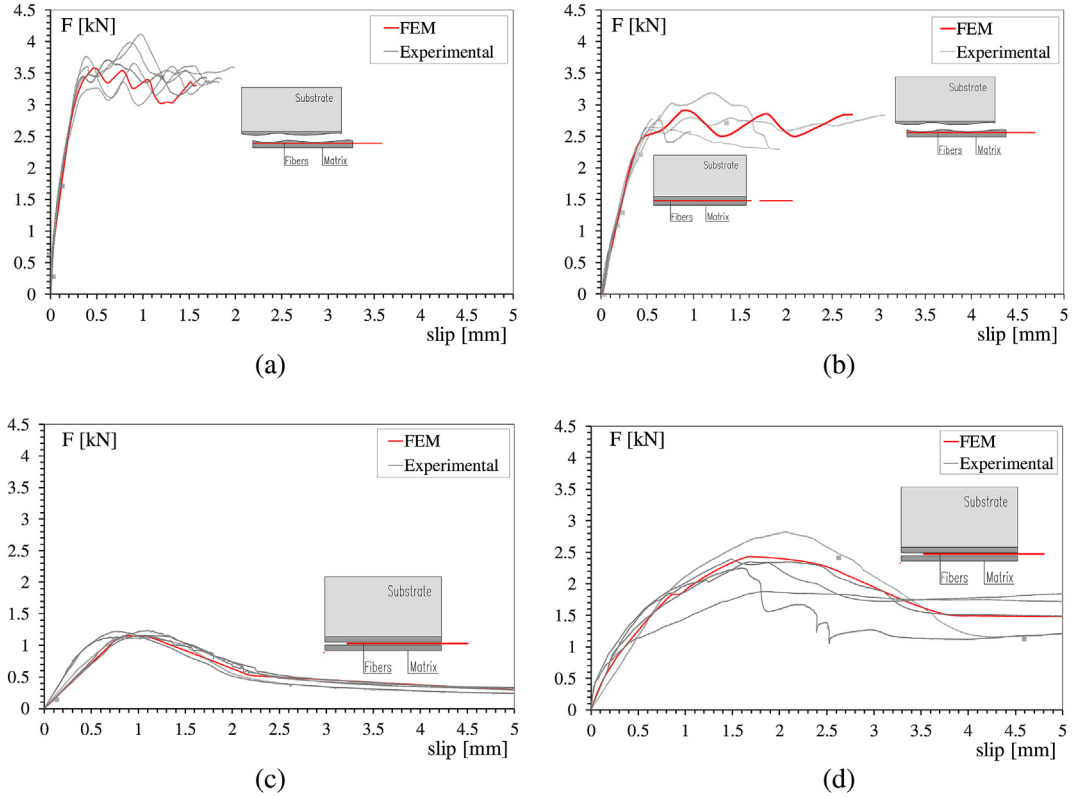

Fig. 6. Results of experimental bond test performed on the four different types of strengthening systems and comparison with numerical (FEM) model: (a) Type CP; (b) Type GP; (c) Type CD; (d) Type GC.

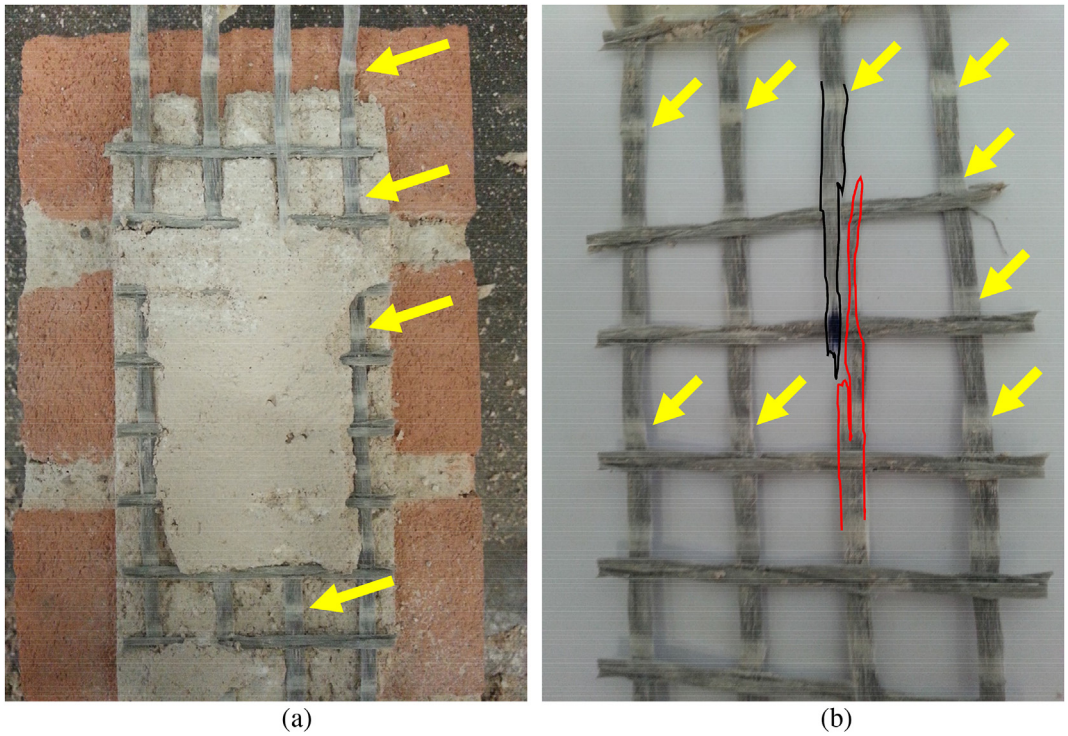

Fig. 7. Details of the inspection performed at the end of bond test on the GC sample reaching the lowest peak load. The arrows indicate the original connections positions (i.e. light gray spots on the longitudinal bundles).

tensile tests, the fine mesh of the plane FE model shown in Fig. 9a was adopted to describe the geometry of a longitudinal cross-section. A detailed modelling, through isoparametric four nodes FEs, of the two layers of reinforcement matrix and the embedded composite fiber layer was performed. The three layers were connected by two non-linear fiber-matrix interfaces in order to introduce the possible relative displacement between them. Similarly, the refined mesh illustrated in Fig. 9b was adopted to describe the geometry of a longitudinal cross-

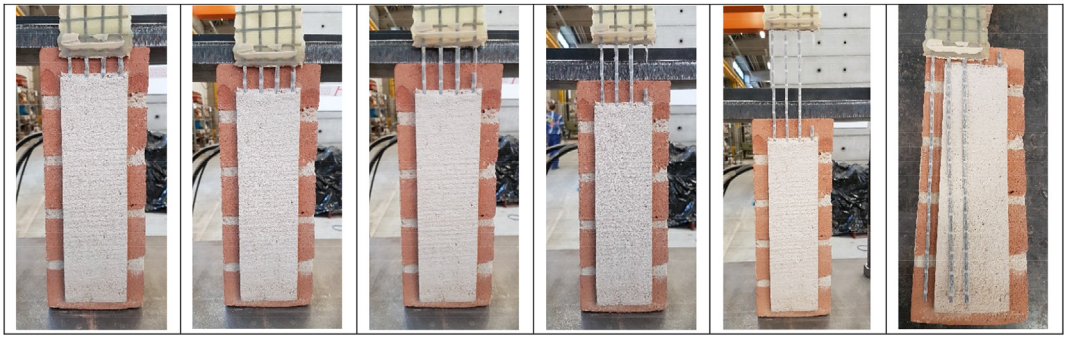

Fig. 8. Sequence of the various steps with increasing fibers slippage until the complete pullout of GC specimen during a bond test.

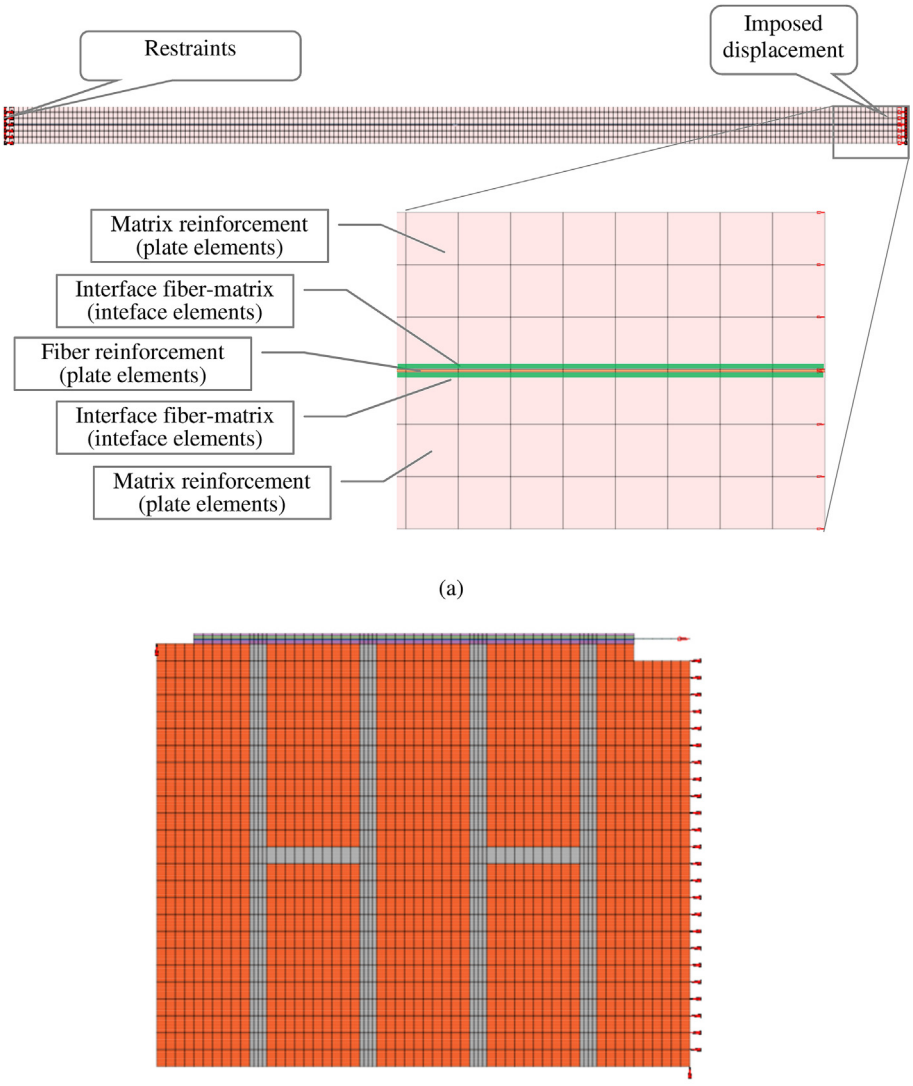

Fig. 9. Finite element models adopted for the study of FRCM system: (a) Tensile test with detail of the five layers modelling the reinforcement; (b) Bond test.

section of the specimens subjected to single-lap shear tests. The modelling and the numerical analyses were performed with MidasFEA software [35], considering static loading conditions.

The properties of the materials were introduced as obtained from experimental tests (see Tables 1 and 2). A smeared total strain crack model [36] was considered for the simulation of damage inside the mortar both in tension and compression states. The equivalent length $h = 2.8$ mm, governing the fracture process, was calibrated by following indications provided by Rots [37]. Material degradation was introduced in the mortar by considering a post peak exponential decay in tension and an elastic-plastic stress-strain relation under compression.

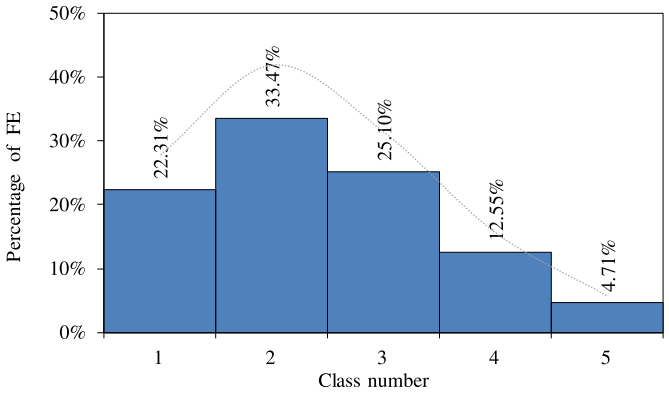

Fig. 10. Randomization of the cracks position: Percentage Poisson's distribution of the FE associated to each one of the five classes of reinforcement matrix.

4.2. Randomization of the cracking phenomena

It is well known that the first crack along elements made of unreinforced brittle materials (i.e. cementitious mortar), subject to uniform axial loading conditions, will localize in the cross-section having the lowest tensile strength. Correspondingly, it is not possible to define *a priori* a statistical distribution of the tensile strength along all the possible cross-sections, and the only physical measure available after each test will be the smallest strength value.

In the present study, in order to introduce in a random way the cracks position (connected to unavoidable defects and tensile strength variability of the reinforcement mortar), for the tensile strength, five different mortar classes have been defined following a Poisson distribution. One of the five classes, and its mechanical properties, has been randomly assigned at every FE of the matrix. Fig. 10 shows the distribution of the percentage of FEs belonging to each of the five classes *vs* the class number. A Poisson distribution of the number of FEs having a given mortar tensile strength with a number of events $n = 5$ and a mean value of the events $\lambda = 1.5$ was adopted for all the numerical models used to reproduce the experimental results in the following. The fracture energy, the compressive and tensile strengths adopted for the different classes of mortar, obtained from experimental outcomes are reported in Table 5, together with the elastic modulus *E*. In particular, tensile fracture energy of mortar used for CP-GP cases has been amplified by 5 times in order to take into account the contribution of the adhesion promoter, according to experimental outcomes.

4.3. Calibration of τ-slip curve

The adoption of a properly assessed τ-slip relation is maybe the fundamental aspect for a correct numerical interpretation of the experimental outcomes emerging from FRCM tests. In fact, by changing the shape of bond-slip relation, the failure mechanism can be strongly modified. This stage of the work has been approached by considering two main steps: (i) the establishment of the type of failure to reproduce and (ii) the numerical calibration of the most suitable bond-slip relation.

As far as the first step is concerned, the most typical failure mechanism was reproduced for each class of FRCM, according to experimental results. With reference to Fig. 1, for CP and GP classes, a failure mode III was assumed while for CD and GC, a failure mode IV was considered. From an accurate post-test inspection on samples adopting the adhesion promoter, very specific aspects emerged in terms of local behavior. As first, since the failure mechanism III developed inside a layer of matrix, it must be a failure involving the shear strength of the mortar. In more details, the delamination surface has been localized in correspondence of the penetration depth of the adhesion promoter used to impregnate the reinforcement grid. As second, the delamination phenomena produced an apparent dented surface in correspondence of the transverse mortar bed joints of the wall panel, as if the different type of substrate (clay or mortar) could influence the penetration depth (see Fig. 11a). Because of the latter, a different bond-slip relation was attributed at the interface elements localized in correspondence of masonry joints, so to differentiate the behavior from that of interface elements localized in correspondence of bricks (Fig. 11b). In this way, the experimental wavy behavior of the last branch of the curves provided by this type of strengthening systems during bond-tests has been accurately reproduced.

As far as the second step is concerned, starting from available experimental results, a local bond-slip relation has been obtained for each FRCM class. The application of the so-called direct method [38], based upon measures of local bond stress and fiber strains, presents some practical difficulties in the case of FRCM materials [39]. Therefore, in the present paper, the calibration of the local τ-slip relation, for each FRCM class, has been obtained starting from the experimental global force-slip curve by means of an inverse analysis by adopting, for the sake of simplicity, a multilinear five branches τ-slip relation. For each class, by considering four different topologies (i.e. four topologies obtained by considering different random attribution of reinforcement mortar properties) for the numerical model, an iterative procedure allowed to evaluate the values that minimize the distance between the experimental findings and numerical predictions. It was performed, for samples of the same class, with a least square method, and allowed to evaluate the mean values summarized in Table 6 generating the τ-slip relations showed in Fig. 12. The last sub-horizontal branch of the bond law allows inserting also the friction force [40] contribution that same classes of samples showed during the debonding phase. The obtained relations are very similar to those proposed in literature [6], but the adoption of multilinear laws without shape-imposed curve allows a more accurate description of the experimental tests.

4.4. Comparison with bond tests results

4.4.1. CP reinforcement

In Fig. 6a, the curves of the experimental campaign are overlapped to the numerical predictions obtained adopting the mean parameters indicated in Table 6 for the topology producing the best fitting. As can be observed, the initial stiffness is accurately captured, the value of the force at the plateau is comparable on average with the measured force

Table 5
Mechanical properties of the five classes of reinforcement matrix adopted in the modelling in order to introduce a random cracks distribution (f_c: compressive strength; f_t: tensile strength; G_f: fracture energy in tensile state).

Class #	CP - GP				CD - GC			
	f_c [MPa]	f_t [MPa]	G_f [N/mm]	E [GPa]	f_c [MPa]	f_t [MPa]	G_f [N/mm]	E [GPa]
1	0.05	0.01	0.00	8	0.08	0.02	0.00	14
2	3.28	0.63	0.30	8	5.00	0.97	0.06	14
3	6.55	1.27	0.60	8	10.00	1.93	0.12	14
4	9.83	1.90	0.90	8	15.00	2.90	0.18	14
5	13.11	2.53	1.20	8	20.00	3.87	0.24	14

(a)

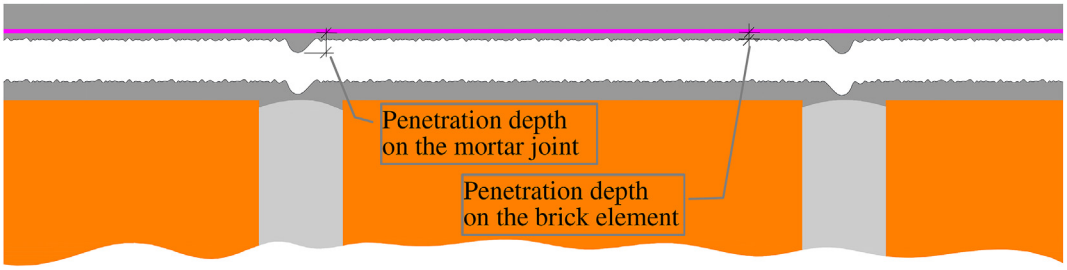

(b)

Fig. 11. Physical vs. numerical interpretation of the behavior of different FRCM systems: (a) Detail of the dig surface experimentally observed for the case of delamination of the inner matrix in presence of the adhesion promoter; (b) Hypothesis of different penetration depth of the adhesion promoter introduced to explain the two different τ-slip relations adopted in the FEM for the different portions FRCM-mortar joint and FRCM-brick.

level and the numerical solution reproduces in a reliable way the wavy behavior of the experimental results, with very similar slip intervals between two consecutive force peaks. After the confirmation that the numerical model is able to describe properly the global behavior of the strengthening systems, it has been used to investigate in detail what happened in terms of local behavior at the mortar-fiber interface, in order to clarify with more accuracy the debonding mechanism causing the final failure. For the CP type of reinforcement, the distribution of shear stress (τ) at the interface during the bond test is reported in Fig. 13 for five increasing slip levels, named *s*1-*s*5 and localized as points in the force-slip global curve of Fig. 13a. At the beginning, for low level of slip, the distribution of the shear stress decreases moving away from the loaded-end (see Fig. 13b). The first force peak of Fig. 13a corresponds to a slip (*s*2) able to activate the maximum bond strength of the first mortar bed-joint added to the whole bond capacity of the following brick (i.e. brick between first and second bed-joint) and to a relevant bond force coming from the second bed-joint (Fig. 13c). Further increasing the slip, the debonding of the initial portion of the specimen (first bed-joint included) makes the force capacity decrease (slip *s*3), until the second bed-joint approaches its maximum bond capacity (tangential stress distribution of Fig. 13d). The following peak of Fig. 13a is attained when the full activation of the second mortar bed-joint is reached, together with the relevant involvement of following bed-joints (Fig. 13e). In general, each peak of Fig. 13a is reached when at least one mortar bed-joint deploys its maximum bond capacity while the local minimum corresponds to the full debonding of the same mortar bed-joint, with the following not yet fully active. This wavy behavior proceeds until new mortar bed-joints are available along the

Table 6
Bond-slip (τ-s) relations adopted in the numerical analyses for the study of the different strengthening systems.

CP reinf-mortar		CP reinf-brick		GP reinf-mortar		GP reinf-brick		CD		GC	
τ [MPa]	s [mm]	τ [MPa]	s [mm]	τ [MPa]	s [mm]	τ [MPa]	s [mm]	τ [MPa]	s [mm]	τ [MPa]	s [mm]
0.0	0.0	0.0	0.0	0.0	0.0	0.0	0.0	0.0	0.0	0.0	0.0
0.15	0.007	0.15	0.007	0.8	0.3	0.8	0.3	0.055	0.7	0.04	0.06
0.7	0.19	0.45	0.19	0.8	0.5	0.0	0.55	0.055	1	0.13	0.6
0.7	0.34	0.0	0.39	0.0	0.95	0.0	0.8	0.025	2.15	0.13	1.5
0.0	0.5	0.0	0.5	0.0	0.99	0.0	0.9	0.02	3.5	0.08	3.2
0.0	1.0	0.0	1.0	0.0	1.0	0.0	1.0	0.014	5.0	0.078	5.0

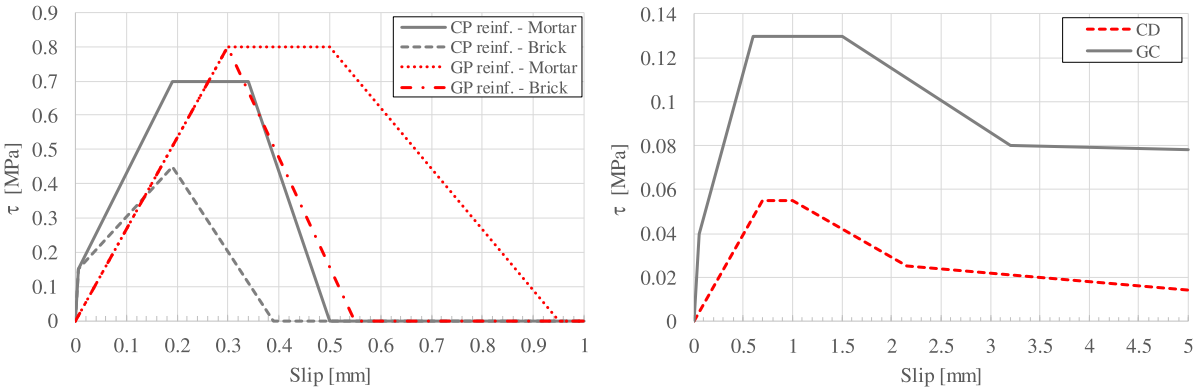

Fig. 12. τ-slip relations obtained from fitting procedure and then adopted in the numerical analyses of FRCM systems: (a) with adhesion promoter; (b) without promoter.

bonded length. The test stops with a brittle failure (*s*5) when an insufficient bond length is left attached to the substrate; at that moment, the bond capacity cannot be fully developed (Fig. 13f). It is important also to notice that the described propagation mechanism is strongly influenced by the cracking pattern developing inside the reinforcement matrix during the loading process. The variability of this process is one of the main sources of considerable dispersion observed among the peak force values recorded during the experimental tests. In general, the slip increments between two consecutive peaks are properly predicted by the numerical model leading to the four peaks usually observed during the tests (Fig. 6a). Following the criteria indicated in Ref. [11] based on the stress transfer zone, the effective bond length l_{eff} can be estimated for this class of specimens in the 80–100 mm range.

4.4.2. GP reinforcement

In this case, the situation is quite different with respect to the carbon grid of CP reinforcement class. In fact, as described in a previous section, the failure mode of the present strengthening system is mainly connected to a progressive fraying of the grid fibers (with few amount of real slip) in four of the tested specimens and presents delamination just in one case. Therefore, for this reinforcement class the strength capacity of the fibers is comparable to delamination capacity and so it is not simple to assess, in general, which one of the two mechanisms will govern the failure. In the curves of Fig. 6b, the real bond slip stopped at about 0.5 mm while the rest of the measured slip is to be attributed to fibers damaging, where this type of damaging mechanism was not introduce in FE model. Therefore, the bond-slip relations were calibrated based on the only sample failed due to delamination, with the force-slip curve showing a wavy behavior before the complete detachment. Even for this class of FRCM, the obtained global results are satisfying. For this class of reinforcement the effective bond length l_{eff} is comparable to the CP case.

4.4.3. CD reinforcement

As discussed before, CD and GC reinforcements exhibited a clear slippage of the longitudinal fibers within the two layers of the reinforcement matrix. In fact, the longitudinal carbon dry fibers completely pulled out from the layers of mortar, leaving intact the transversal fibers. Therefore, the initial stiffness of the τ-*s* curve would be sufficiently low (see Table 6) and its post peak behavior will show a residual bond capacity, governed by friction contribution. The experimental behavior is properly matched by the numerical curve (Fig. 6c). The poor adhesion between dry fibers and mortar leads to a value of τ_{max} smaller than the value reported in Table 6 for GP and CP strengthening systems and to a larger compliance. Consequently, the maximum bond capacity of this system is considerably reduced if compared to previous cases. In this case, the absence of a plateau in the global force-slip curve makes the bond length l_{eff} not well defined. In fact, in the global curve, at the peak point all the reinforcement length represents an active transfer zone and, in general, is not possible to define whether increasing the length of the specimens the peak load value increase or not, but in general l_{eff} should be 250 mm or even more.

4.4.4. GC reinforcement

GC strengthening system, characterized by a coated glass grid without an adhesion promoter, exhibited an experimental behavior similar to CD reinforcement. With reference to the latter, GC reinforcement reached an higher peak force (about double); then its force-slip curve is characterized by a stiffer initial branch and an higher value of residual friction force. Even in this case, the contribution of the transverse fibers to the total strength of the system seems negligible. In Fig. 6d the numerical curve has been overlapped to the experimental ones, showing, also in this case, as the τ-*s* relation properly calibrated for the case at hand, allows capturing the general features of the system. The adoption of a coated reinforcement grid improves the performance of the system with respect to the adoption of dry fibers, but seems not sufficient to achieve the performance of the systems with an adhesion promoter.

Shapes and values of the τ-*s* relations here proposed produce a good matching between numerical and experimental results, allowing also a comparison of the bond performances of the different types of reinforcements considered.

4.5. Tensile tests

As far as the tensile tests are concerned, the numerical curves obtained by FE models with the topology showing the best fitting of experimental data are reported in Fig. 4, for all the four considered cases.

4.5.1. CP reinforcement

The numerical curve follows the same phases identified during the experimental tests: (i) an elastic branch concluded by the appearance of the first micro-cracks; (ii) increasing the elongation, the number of cracks grows and stabilizes (between 16 and 20 detected during the tests) and finally (iii) the cracks opening increases without the introduction of new ones, until the tensile failure of the fibers. The curve is very smooth, in agreement with experimental tests, and presents a

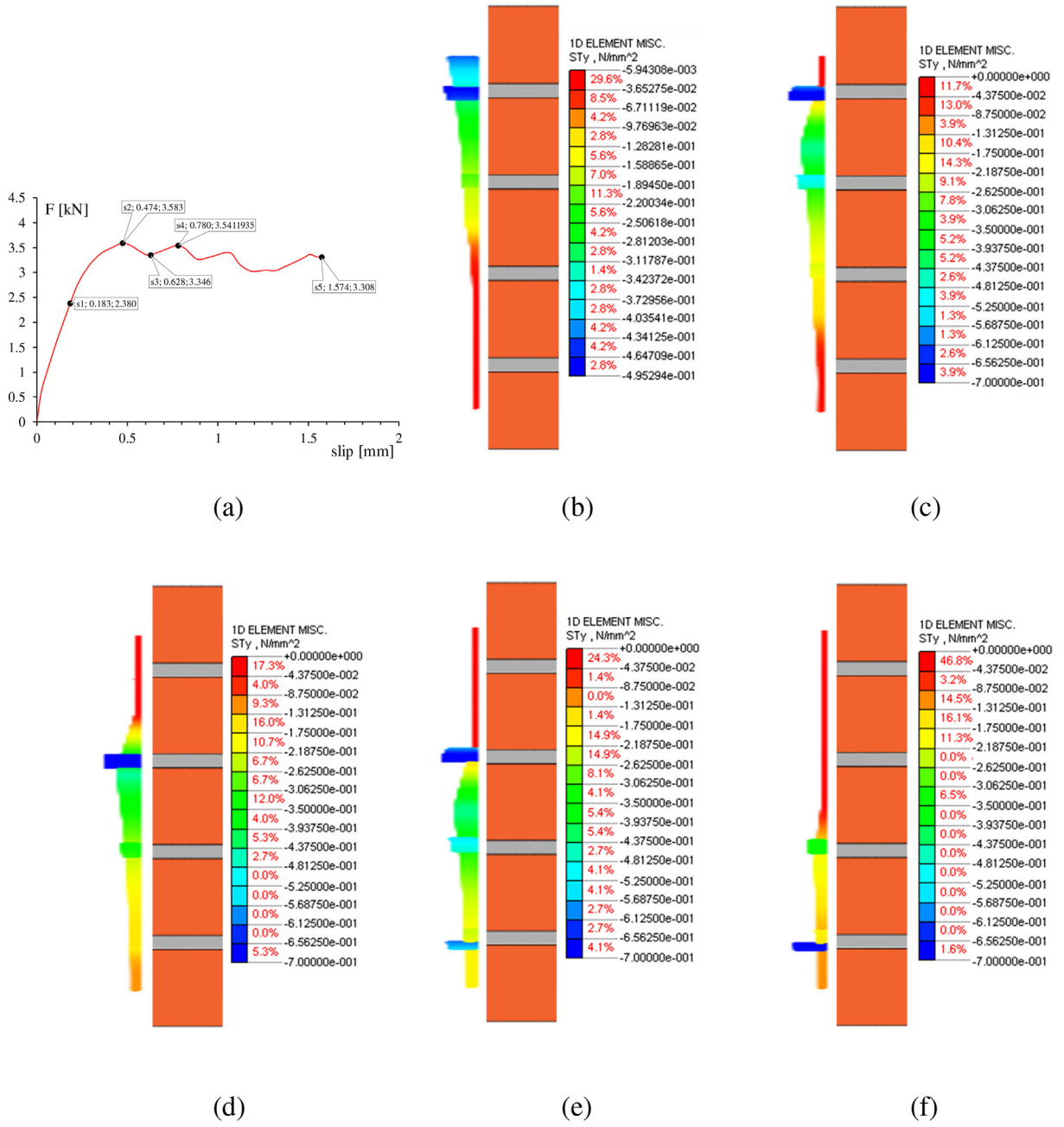

Fig. 13. Distribution of shear stress (τ) obtained during the numerical analysis performed on CP reinforcement for the increasing slip levels labelled s1-s5 in (a) and respectively depicted from (b) to (f).

continuous transition between phases (i) and (ii). This effect, mechanically related to the capacity of the adhesion promoter to penetrate into the matrix and apparently, to increase the ductility of the material, has been numerically obtained by increasing the tensile fracture energy of the mortar. In fact, the system is able to keep transmitting the force, with negligible slip discontinuity, also in correspondence of a crack.

4.5.2. GP reinforcement

The comparison between experimental and numerical results is reported in Fig. 4b. A good matching can be observed. The qualitative behavior of the curves related to CP and GP reinforcements is quite similar since they share the introduction of the same adhesion promoter. During the cracking phase (during the tests 10 to 14 cracks were identified), a smaller tension stiffening effect can be observed. These aspects are captured in a suitable way by the model, also by considering a smeared crack model for computing the damaging of the specimens.

4.5.3. CD reinforcement

As introduced in the previous section, for this class of reinforcement, the experimental curves result very scattered and sawtoothed when cracks open. The load drops are produced by the noticeable slip between the mortar and the reinforcement grid at the crack appearance. The load is then recovered through the shear stress transfer mechanism, starting from the crack edges. CD reinforcements present the first crack at a strain level of 0.02%, followed by further secondary cracks (about 3–6 main cracks observed during the tests) appearing at a later stage. The fundamental role played by the first crack is related to the small fracture energy characterizing the shear constitutive behavior. In addition, in this case, as showed in Fig. 4c, the numerical model provides for a good matching with experimental results. The prediction is not so

accurate in the description of the second branch, due to the adoption of a smeared crack damage model, which is not fully adequate to reproduce brittle phenomena with localized cracks.

4.5.4. GC reinforcement

The comparison between experimental and numerical results from tensile test is reported in Fig. 4d. After the onset of cracking, the glass fibers reinforced specimens show the appearance of a larger number of cracks (between 5 and 8 identified during the tests), characterizing a more pronounced tension-stiffening effect. The crack stabilization phase starts after a deformation of about 0.4% and is mainly governed by the reinforcement grid axial stiffness. The numerical stress-strain curve properly matches the experimental features; moreover, the smeared crack approach seems to be more suitable to describe brittle phenomena with larger fracture energy (cracks better dispersed along the specimen).

This is a further confirmation that, in general, the simplified FE model seems able to represent the general features of the tests, both for glass and carbon specimens, producing numerical results in good agreement with the experimental outcomes. It is important to highlight that the adoption of interface elements, introducing the possible slip between the various layers of reinforcement, is necessary in order to capture in a realistic way the global behavior of the FRCM samples also in tensile tests.

Furthermore, as already discussed for bond tests, in order to prove the ability of the FE models to reproduce in a suitable way the behavior of reinforcement systems and to verify the role played by the mortar strength variability, the correspondence between experimental results and numerical outcomes has been investigated also in terms of local behavior. In particular, the number of cracks developed during the tests have been compared. Fig. 14 shows the contour plot of the longitudinal strain pattern at failure of the four different types of reinforcement system, according to the mortar properties distribution used to evaluate curves in Fig. 4. Strain patterns of CP and GP type of reinforcement, reported respectively in Fig. 14a and b, show a number of cracks (19 for CP and 16 for GP type) comparable to the values observed during the tests. With respect to CD and GC types of strengthening systems, the number of cracks considerably reduces, ranging between 4 and 8, respectively for CD and GC systems. These quantities result in full agreement with the experimental count. This suggest that the Poisson's distribution adopted in the numerical simulation for tensile cracking provides for suitable results for the study of the investigated problem.

4.6. Evaluation of the effects of random attribution of mortar properties on global curves

In order to prove the reliability and stability of the numerical model when varying its topology (i.e. the properties of the reinforcement mortar), the main results in terms of global curves are here reported, for the sake of brevity, for two cases. CP class of specimens was considered for bond test, while GP class was considered for tensile test. By following the described Poisson's distribution of the matrix properties, four different random topologies of matrix were produced. The other material properties, assumed as deterministic, are those obtained by preliminary characterization tests (Tables 1 and 2) and reported in Table 6 for τ-slip relations. Through numerical analysis, they provided for the curves reported in Fig. 15, where the corresponding envelope of experimental results (grey area) is also reported. The four numerical curves in Fig. 15a show a wavy behavior oscillating inside the range of the experimental results with similar features and values but with a lower dispersion of results. This could be because a number of parameters were considered as deterministic in the model while they can vary in real tests. Also in the case of tensile tests (see Fig. 15b), the numerical results exhibit an excellent agreement with experimental tests, again with a lower dispersion of the curves. It seems important to notice that the numerical solutions are always included inside the grey region, between the lower and the upper experimental boundary. In general, the experimental-numerical comparison is very good. Furthermore, the outcomes dispersion is of the same order of magnitude of the experimental one, thus confirming also the suitability of the Poisson's distribution for the description of matrix properties variability.

5. Concluding remarks

The paper presents the results of tensile and single-lap bond tests carried out on FRCM composites based on different types of carbon and glass grids, coupled with two different types of natural hydraulic lime matrices. Four different strengthening systems were considered, trying to cover as much as possible the current wide scenario of available different strengthening solutions. Two different types of mortar coupled with dry carbon, coated glass, impregnated glass and impregnated carbon bi-directional grids were considered in the experimental tests. In order to improve the adhesion between the fibers and the matrix, an adhesion promoter was used in some cases. The different classes of systems were selected in order to produce different failure scenarios, cracking propagations and adhesion mechanisms. The outcomes can be considered as limit cases of the range of possible results expected by current FRCM applications.

Crack patterns and failure modes of GFRCM and CFRCM strengthening systems subjected to tensile and bond tests were discussed and analyzed, particularly on a global scale. The role of adhesion promoter and fibers coating were found to be particularly relevant in the definition of the general performance of the different systems.

In order to investigate the local behavior of each single component and of the corresponding interfaces, detailed 2D finite element models were introduced. This allowed for the definition of local τ-slip curves at the matrix-fiber interface and allowed a deeper understanding of the various experimental scenarios.

The smeared total strain crack model introduced to describe the matrix behavior was found to be appropriate for systems characterized by a good adhesion between fibers and matrix. Randomization of the tensile strength of the matrix, according to a Poisson distribution, led to satisfactorily results, confirming also the suitability of this type of distribution.

The matrix mortar tensile strength obtained via three-point flexure tests and direct tensile tests was found to be quite different, with a ratio of about two. Values obtained through the latter seem in better agreement with the experimental outcomes coming from FRCM tensile tests. Further investigations are needed to clarify this aspect and to standardize the test procedure (relevance of the $40 \times 40 \times 160\,mm^3$ mortar specimens).

Bond capacity at the matrix-fiber interface has been proved to be strongly affected by the presence of the adhesion promoter, reducing the scattering of results from tensile tests and producing a specific geometry of the delaminated matrix surface. In particular, a dented shape was observed in correspondence of the transversal mortar bed-joints of the masonry panel, suggesting that the type of surface on which the strengthening system was applied influenced the penetration depth of the adhesion promoter. Therefore, a different bond-slip relation was attributed to the interface elements located in correspondence of mortar bed-joints. As a result, an excellent correspondence between experimental and numerical results was found.

For the considered cases, the role of the transverse bundles during bond tests was found to be negligible, since they detached or slipped with respect to the longitudinal bundles. Therefore, the considered 2D FE models seems able to represent the general features of the tests. In any case, the shape of the calibrated τ-slip relations (multilinear with 5 branches) implicitly also takes into account the possible role of transversal bundles. These interface relationships clarified the role of the fibers coating and of the friction between the matrix and the fibers, allowing for an accurate representation of the failure mechanisms experimentally observed.

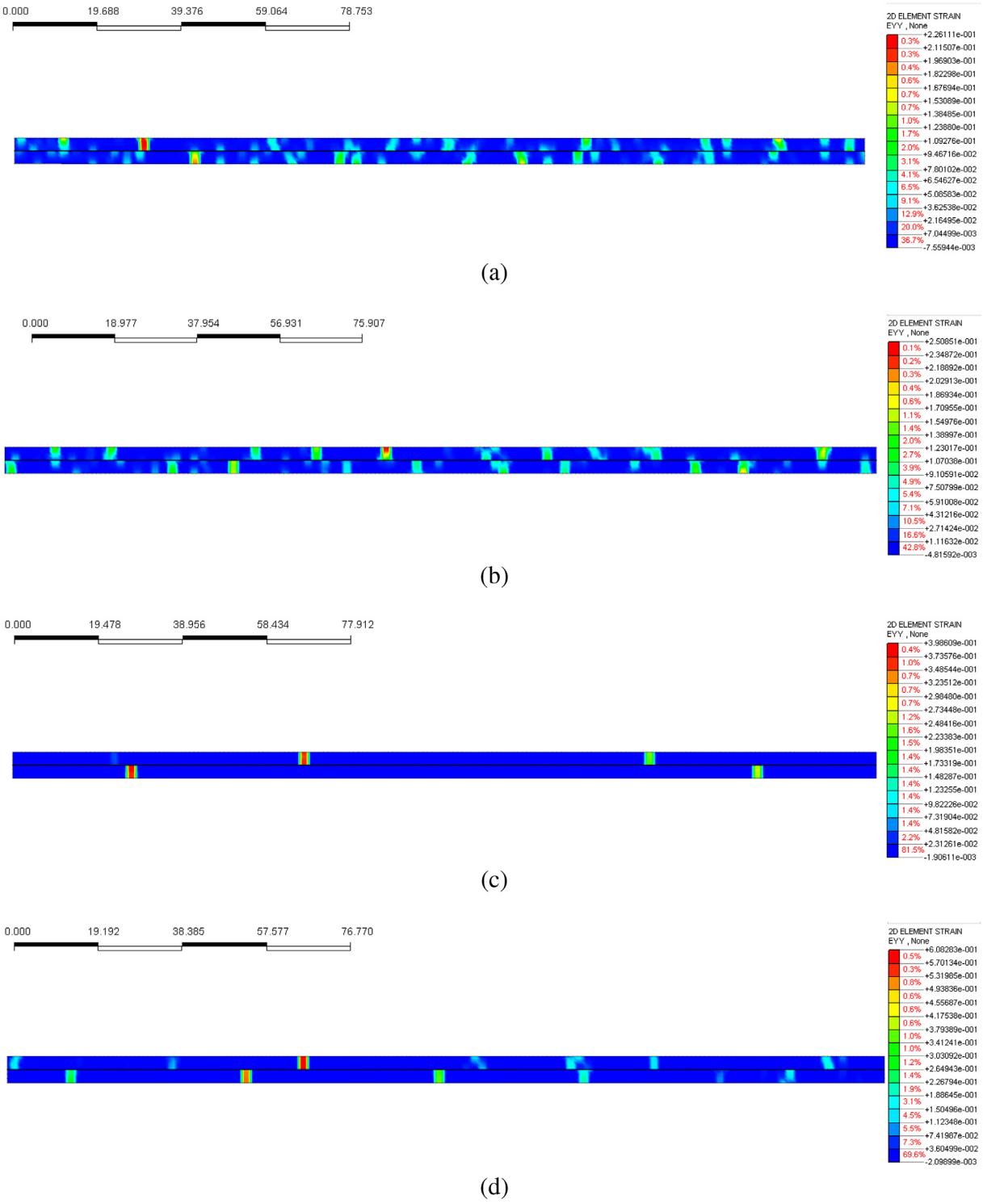

Fig. 14. Numerical longitudinal strain contour for tensile tests at failure: (a) CP; (b) GP; (c) CD; (d) GC reinforcement.

The comparison between numerical and experimental results from tensile tests showed the capability of FE models to reproduce in a suitable way both the global and the local behavior of the FRCM specimens, for all the different types of strengthening systems considered. In particular, the effect of the variation of mechanical properties of the mortar (different topologies) was investigated, clarifying its importance in the definition of the experimental scattering. Only the adhesion promoter was able to modify the behavior of the system, introducing a gradual transition between the uncracked and the cracked phase of the mortar and considerably reducing the slip among fibers and matrix.

It is important to notice that the adoption of interface elements introducing the possible slip between fibers and matrix is necessary in order to properly capture the global behavior of the FRCM sample subject to tensile tests.

The experimental results presented and the numerical analysis developed clearly remark the fundamental importance of the compatibility between the two materials (fibers and matrix), which have to work together as a system. In this framework, and for the materials considered, less importance could be given to the mechanical properties of the single constituent or of the substrate. At the same time, the

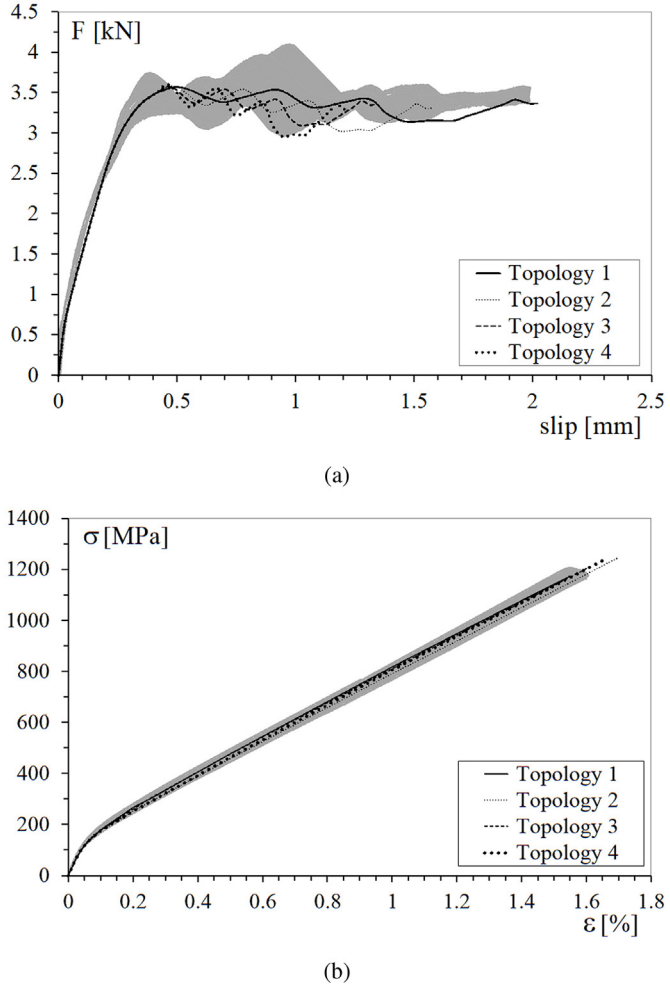

Fig. 15. Results obtained by considering four different FE mesh topologies of the properties of the reinforcement mortar: (a) CP reinforcement in bond tests; (b) GP reinforcement in tensile tests. Shadowed areas are the experimental envelopes.

mechanical interlock contribution, possibly provided by fibers bundles orthogonal to the direction of the applied force, seems to be not relevant since those bundles, in most of the cases, slide with respect to the longitudinal bundles.

Acknowledgements

The financial support of (Italian) Department of Civil Protection (ReLUIS 2018 Grant – Innovative Materials) is gratefully acknowledged. The authors would like also to thank Ardea Progetti e Sistemi S.r.l. and G&P Intech S.r.l. for providing materials.

Appendix A. Supplementary data

Supplementary data to this article can be found online at https://doi.org/10.1016/j.compositesb.2018.12.115.

References

[1] Butler M, Mechtecherine V, Hemplel S. Durability of textile reinforced concrete made with AR glass fibre: effect of matrix composition. Mater Struct 2010;43:1351–68.
[2] De Santis S, de Felice G. Tensile behaviour of mortar-based composites for externally bonded reinforcement systems. Composites Part B 2015;68:401–13.
[3] D'Ambrisi A, Feo L, Focacci F. Experimental and analytical investigation on bond between Carbon-FRCM materials and masonry. Composites Part B 2013;46:15–20.
[4] de Felice G, De Santis S, Garmendia L, Ghiassi B, Larrinaga P, Lourenco PB, Oliveira DV, Paolacci F, Papanicolaou CG. Mortar-based systems for externally bonded strengthening of masonry. Mater Struct 2014;47(12):2021–37.
[5] Carozzi FG, Bellini A, D'Antino T, De Felice G, Focacci F, Hojdys L, Laghi L, Lanoye E, Micelli F, Panizza M, Poggi C. Experimental investigation of tensile and bond properties of Carbon-FRCM composites for strengthening masonry elements. Composites Part B 2017;128:100–19.
[6] Caggegi C, Carozzi FG, De Santis S, Fabbrocino F, Focacci F, Hojdys L, Lanoye E, Zuccarino L. Experimental analysis on tensile and bond properties of PBO and aramid fabric reinforced cementitious matrix for strengthening masonry structures. Composites Part B 2017;127:175–95.
[7] De Santis S, Ceroni F, de Felice G, Fagone M, Ghiassi B, Kwiecień A, Lignola GP, Morganti M, Santandrea M, Valluzzi M, Viskovic A. Round Robin test on tensile and bond behavior of steel reinforced Grout systems. Composites Part B 2017;127:100–20.
[8] Leone M, Aiello MA, Balsamo A, Carozzi FG, Ceroni F, Corradi M, Gams M, Garbin E, Gattesco N, Krajewski P, Mazzotti C, Oliveira D, Papanicolaou C, Ranocchiai G, Roscini F, Saenger D. Glass fabric reinforced cementitious matrix: tensile properties and bond performance on masonry substrate. Composites Part B 2017;127:196–214.
[9] Ombres L. Analysis of the bond between fabric reinforced cementitious mortar (FRCM) strengthening systems and concrete. Composites Part B 2015;69:418–26.
[10] D'Ambrisi A, Feo L, Focacci F. Experimental analysis on bond between PBO-FRCM strengthening materials and concrete. Composites Part B 2013;44:524–32.
[11] D'Antino T, Colombia P, Carloni C, Sneed LH. Estimation of a matrix-fiber interface cohesive material law in FRCM concrete. Compos Struct 2018;193:103–12.
[12] Capozucca R. Experimental FRP/SRP-historic masonry delamination. Compos Struct 2010;92:891–903.
[13] Carrara P, Ferretti D, Freddi F. Debonding behavior of ancient masonry elements strengthened with CFRP sheets. Composites Part B 2013;45:800–10.
[14] de Felice G, Aiello MA, Bellini A, Ceroni F, De Santis S, Garbin E, Leone M, Lignola GP, Malena M, Mazzotti C, Panizza M, Valluzzi MR. Experimental characterization of composite-to-brick masonry shear bond. Mater Struct 2016;49:2581–96.
[15] Mazzotti C, Ferracuti B, Bellini A. Experimental bond tests on masonry panels strengthened by FRP. Composites Part B 2015;80:223–37.
[16] Bellini A, Mazzotti C. A review on the bond behavior of FRP composites applied on masonry substrates. RILEM Technical Letters 2017;2:74–82.
[17] Ceroni F, Leone M, Rizzo V, Bellini A, Mazzotti C. Influence of mortar joints on the behaviour of FRP materials bonded to different masonry substrates. Eng Struct 2017;153:550–68.
[18] Sassoni E, Andreotti S, Bellini A, Mazzanti B, Bignozzi MC, Mazzotti C, Franzoni E. Influence of mechanical properties, anisotropy, surface roughness and porosity of brick on FRP debonding force. Composites Part B 2017;108:257–69.
[19] Sassoni E, Sarti V, Bellini A, Mazzotti C, Franzoni E. The role of mortar joints in FRP debonding from masonry. Composites Part B 2018;135:166–74.
[20] Arboleda D, Loreto G, De Luca A, Nanni A. Material characterization of fiber reinforced cementitious matrix (FRCM) composite laminates. Proceedings for 10th international symposium on ferrocement and thin reinforced cement composite. 2012. [Havana].
[21] Donnini J, Corinaldesi V, Nanni A. Mechanical properties of FRCM using carbon fabrics with different coating treatments. Composites Part B 2016;88:220–8.
[22] Carloni C, Verre S, Sneed LH, Ombres L. Loading rate effect on the debonding phenomenon in fiber reinforced cementitious matrix-concrete joints. Composites Part B 2017;108:301–14.
[23] Zhu D, Peled A, Mobasher B. Dynamic tensile testing of fabric-cement composites. Constr Build Mater 2011;25:385–95.
[24] Awani O, El-Maaddawy T, Ismail N. Fabric-reinforced cementitious matrix: a promising strengthening technique for concrete structures. Constr Build Mater 2017;132:94–111.
[25] Donnini J, Corinaldesi V. Mechanical characterization of different FRCM systems for structural reinforcement. Constr Build Mater 2017;145:565–75.
[26] Carozzi FG, Poggi C. Mechanical properties and debonding strength of Fabric Reinforced Cementitious Matrix (FRCM) systems for masonry strengthening. Composites Part B 2015;70:215–30.
[27] Capozucca R. Effects of mortar layers in the delamination of GFRP bonded to historic masonry. Composites Part B 2013;44:639–49.
[28] Lignola GP, Caggegi C, Ceroni F, De Santis S, Krajewski P, Lourenço PB, Morganti M, Papanicolaou C, Pellegrino C, Prota A, Zuccarino L. Performance assessment of Basalt FRCM for retrofit applications on masonry. Composites Part B 2017;128:1–18.
[29] D'Antino T, Carloni C, Sneed LH, Pellegrino C. Matrix-fiber bond behavior in PBO FRCM composites: a fracture mechanics approach. Eng Fract Mech 2014;117:94–111.
[30] Bellini A, Ferracuti B, Mazzotti C. Effect of matrix on bond between FRCM and masonry. Proc. Of FRPRCS-12 & APFIS-2015 joint conference, Nanjing, China. December 2015. p. 14–6.
[31] Lourenço PB, van Hees R, Fernandes F, Lubelli B. Characterization and damage of brick masonry. Costa A, Guedes J, Varum H, editors. Structural rehabilitation of old buildings. Building pathology and rehabilitation, vol. 2. Berlin, Heidelberg: Springer; 2014.
[32] Mazzotti C, Sassoni E, Bellini A, Ferracuti B, Franzoni E. Strengthening of masonry elements by FRP: influence of brick mechanical and microstructural properties. Key Eng Mater 2015;624:330–7.
[33] UNI-EN 1015-11 Methods of test for mortar for masonry - Part 11: determination of flexural and compressive strength of hardened mortar. 2007.
[34] CNR-DT 215/2008 Istruzioni per la progettazione, l'esecuzione ed il controllo di interventi di consolidamento statico mediante l'utilizzo di compositi fibrorinforzati

a matrice inorganica. 2018. [in Italian].
[35] MidasFEA. Midas FEA user's manual. 2017manual.midasuser.com/EN_Common/FEA.
[36] Rots JG, Nauta P, Kusters GMA, Blaauwendraad J. Smeared crack approach and fracture localization in concrete. Heron 1985;30(1):3–48.
[37] Rots JG. Computational modeling of concrete fracture PhD Dissertation Delft, Netherlands: Delft University of Technology; 1988.
[38] Focacci F, D'Antino T, Carloni C, Sneed LH, Pellegrino C. An indirect method to calibrate the interfacial cohesive material law for FRCM-concrete joints. Mater Des 2017;128:206–17.
[39] D'Ambrisi A, Feo L, Focacci F. Bond-slip relations for PBO-FRCM materials externally bonded to concrete. Composites Part B 2012;43:2938–49.
[40] Carozzi FG, Colombi P, Fava G, Poggi C. A cohesive interface crack model for the matrix–textile debonding in FRCM composites. Compos Struct 2016;143:230–41.